Journal of ELECTRONIC MATERIALS, Vol. 49, No. 9, 2020
https://doi.org/10.1007/s11664-020-07996-0

TOPICAL COLLECTION: 18TH CONFERENCE ON DEFECTS (DRIP XVIII)

Influence of Crystallographic Orientation on Schottky Barrier Formation in Gallium Oxide

ROMAN YATSKIV,[1,2] STANISLAV TIAGULSKYI,[1] and JAN GRYM[1]

1.—Institute of Photonics and Electronics of the Czech Academy of Sciences, Chaberka 1014/57, 18251 Prague, Czech Republic. 2.—e-mail: yatskiv@ufe.cz

Highly rectifying graphite/β-Ga_2O_3 Schottky junctions have been prepared by a simple low-cost drop-casting process. The influence of two different crystal orientations on the current transport mechanism in the graphite-based Schottky junctions was investigated by direct-current (DC) and alternating-current (AC) electrical measurements. The nonideal behavior observed for both $\langle\bar{2}01\rangle$ and $\langle 010\rangle$ crystallographic orientations can be explained by the lateral inhomogeneity of the junction related to the imperfection of the graphite/semiconductor interface. A lower density of interface states and their shorter time constants are reported for Schottky junctions formed on $\langle\bar{2}01\rangle$ crystallographic plane, as reflected also by the higher effective barrier height and lower ideality factor.

Key words: Gallium oxide, Schottky barrier diode, graphite/β-Ga_2O_3, $\langle\bar{2}01\rangle$, $\langle 010\rangle$

INTRODUCTION

Gallium oxide (Ga_2O_3) has been widely investigated as a promising material for different electronic and optoelectronic applications such as solar-blind photodetectors, high-voltage devices in power electronics, gas sensors, or scintillators for the detection of nuclear radiation.[1,2] All of these applications require preparation of high-quality thermally stable Schottky contacts. In recent years, different metal schemes have been employed to fabricate Schottky contacts on Ga_2O_3.[3–9] In most cases, the effective barrier height and ideality factor of the Schottky junctions were extracted from the linear portion of the current–voltage (*I–V*) characteristics by using ideal thermionic emission theory. The typical barrier heights and ideality factors lie in the range of 1 eV to 1.6 eV and 1 to 1.7, respectively. However, for oxide semiconductors, the quality of the Schottky contact can be strongly affected by a variety of factors such as residual impurities, crystal defects, and chemical reactions forming oxides and eutectics.[10] The highly asymmetric monoclinic crystal structure of β-Ga_2O_3 leads to strong anisotropy of the thermal conductivity (with values of $11\ m^{-1}\ K^{-1}$, $29\ m^{-1}\ K^{-1}$, and $21\ W\ m^{-1}\ K^{-1}$ along $\langle 100\rangle$, $\langle 010\rangle$, and $\langle 001\rangle$ directions[11]) and optical[12,13] properties for different surface orientations. Anisotropy of electrical properties was also reported;[14] however, this statement is rare, and electrical properties are mostly uniform along the principal crystallographic orientations. Moreover, the defect density in Ga_2O_3 also varies strongly on different surfaces. Defects, such as voids and dislocations in certain crystallographic directions, lead to increased leakage currents in Ga_2O_3 Schottky diodes.[15] Consequently, the anisotropy of the properties has a strong impact on the formation of Schottky barriers. Nevertheless, comparative studies of the electrical properties of Schottky diodes on different crystallographic planes of Ga_2O_3, which are essential for the design of devices, are scarce.[16]

In the work presented herein, the influence of the crystallographic orientation on the behavior of graphite Schottky junctions was studied. The results demonstrate that different crystallographic

(Received October 9, 2019; accepted February 4, 2020;

planes with different properties of the interface between the graphite contact and β-Ga_2O_3 also show different electrical properties.

DEVICE FABRICATION AND MEASUREMENT

Commercially available β-phase Sn-doped Ga_2O_3 substrates with $\langle 010\rangle$ and $\langle \bar{2}01\rangle$ surface orientations were prepared by an edge-defined film-fed growth method (supplied by Tamura Corporation, Japan). According to electrochemical capacitance–voltage profiling, the donor concentration in $\langle 010\rangle$ and $\langle \bar{2}01\rangle$ was 4.4×10^{18} cm^{-3} and 1.1×10^{18} cm^{-3}, respectively. The samples were ultrasonically cleaned in acetone, methanol, and deionized water then dried using N_2 gas. After chemically cleaning the β-Ga_2O_3 wafers using organic solvents, backside ohmic contacts were created using Ga-In alloys. On the front side of each crystallographic orientation, six graphite contacts were fabricated by drop-casting of graphite colloidal solution.[17,18] The properties of the graphite contacts deposited on the different semiconductors have been studied using several techniques, including scanning electron microscopy, x-ray diffraction analysis, and Raman spectroscopy, and the results were reported in our previous paper.[19] The size of the graphite contact for each Schottky contact was measured by optical microscopy. The area of the graphite contact was ~ 0.76 mm^2 (diameter ~ 1 mm). The deviation of the contact size did not exceed 5%. No thermal treatment was used during the preparation of the contact. To extract the fundamental parameters of the diodes, current–voltage (*I*–*V*), capacitance–voltage (*C*–*V*), capacitance–frequency (*C*–*f*), and conductance–frequency (*G*–*f*) measurements were carried out.

The direct-current (DC) electrical properties of the Schottky junctions were studied using a Keithley 237 source measure unit, while the alternating-current (AC) electrical properties were investigated using a Keysight E4990A impedance analyzer. The graphite layer was contacted directly by the measuring probe inside the test chamber.

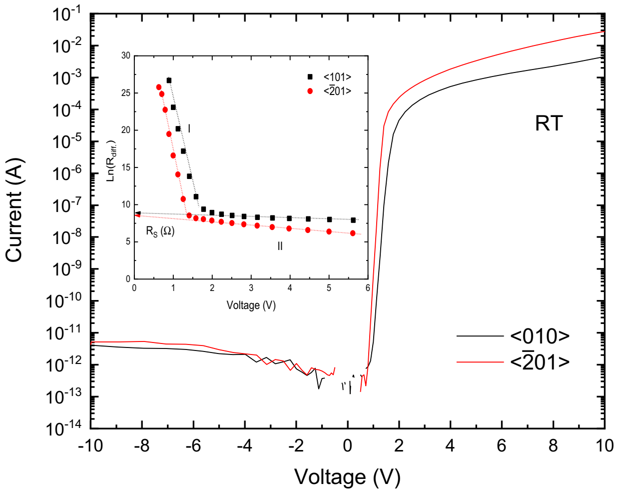

Fig. 1. Representative room-temperature current–voltage characteristics of graphite/Ga_2O_3 junctions for two different surface orientations $\langle 010\rangle$ and $\langle \bar{2}01\rangle$. Inset shows voltage dependence of differential resistance.

RESULTS AND DISCUSSION

All the Schottky barrier diodes exhibited rectifying behavior with a high current rectification ratio of $\sim 1 \times 10^9$ for $\langle 010\rangle$ plane and $\sim 5 \times 10^9$ for $\langle \bar{2}01\rangle$ plane, both measured at ± 10 V. Representative room-temperature *I*–*V* characteristics for both crystallographic orientations are presented in Fig. 1. In the first approach, we used the thermionic emission (TE) model to calculate the basic parameters for the graphite/β-Ga_2O_3 Schottky diodes. According to TE theory, the current–voltage relation can be expressed by the following equation:[20]

$$I = AA^{*}T^{2}\exp\left(-\frac{q}{kT}\phi_{\mathrm{b}}\right)\left[\exp\left(\frac{q(V-IR_{\mathrm{s}})}{\eta kT}\right)-1\right] = I_{\mathrm{s}}\left[\exp\left(\frac{q(V-IR_{\mathrm{s}})}{\eta kT}\right)-1,\right] \tag{1}$$

where I is the current, I_s is the saturation current, A is the diode area, A^* is the effective Richardson constant (41 $\mathrm{A/cm^2\ K^2}$ for Ga_2O_3[9]), q is the electron charge, k is the Boltzmann constant, T is absolute temperature, $\phi_{\mathrm{b}}^{\mathrm{eff}}$ is the effective barrier height, and η is the ideality factor. $\phi_{\mathrm{b}}^{\mathrm{eff}}$ and η were extracted from the linear part of semilog plots according to

$$\eta = \frac{q}{kT}\frac{\mathrm{d}V}{\mathrm{d}(\ln I)}, \tag{2}$$

$$\phi_{\mathrm{b}} = \frac{kT}{q}\ln\left(\frac{AA^{*}T^{2}}{I_{\mathrm{s}}}\right). \tag{3}$$

Deviation of forward *I*–*V* characteristics from exponential behavior is usually attributed to the influence of series resistance. The series resistance was determined from the voltage dependence of the differential resistance under forward bias (Fig. 1, inset).[21]

The results revealed a negligible impact of the different crystallographic planes on the reverse *I*–*V* characteristics. The reverse current saturated for both crystallographic planes with increasing reverse bias, which can be described by the equation[20]

$$I_{\mathrm{rev}} = AA^{*}T^{2}\exp\left(-\frac{q}{kT}\phi_{\mathrm{b}}\right). \tag{4}$$

Table I. Parameters of graphite/β-Ga$_2$O$_3$ Schottky junction obtained from *I–V*, *C–V*, *C–f*, and *G–f* characteristics at room temperature

Parameter	$\langle 010 \rangle$	$\langle \bar{2}01 \rangle$
Mean ϕ_b^{eff} (eV)	1.506	1.553
Standard deviation of ϕ_b^{eff} (eV)	0.030	0.049
Mean ideality factor (η)	1.695	1.339
Standard deviation of η	0.043	0.051
Mean series resistance R_s (kΩ)	8.180	5.999
Rectification ratio at ±10 V, R	1.3×10^9	5.1×10^9
Donor concentration, N_D (cm^{-3})	5.4×10^{17}	1.9×10^{17}
Interface state density, N_{SS} (cm^{-2} eV^{-1})	2×10^{12}	4.2×10^{11}
Time constant, τ (s)	2×10^{-5}	1.7×10^{-7}

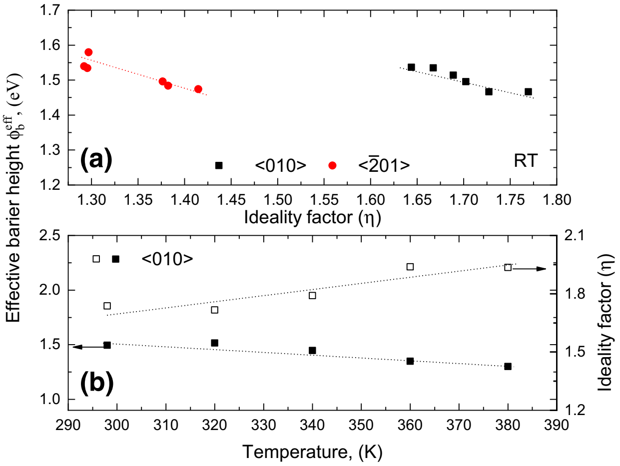

Fig. 2. Relationship between ϕ_b^{eff} and η for Schottky junctions prepared on different crystallographic orientations (a) and representative temperature dependence of ϕ_b^{eff} and η for a particular Schottky junction (b).

For an ideal Schottky barrier, according to Eq. 4, the reverse current for the graphite/β-Ga$_2$O$_3$ is several orders of magnitude lower than the measured experimental data. The real reverse current must be corrected by the effect of the shunt resistance within the whole range of the reverse bias:

$$I^c_{rev} = I_{rev} - {}^{V_{rev}}\!/_{R_{Sh}} \tag{4a}$$

The donor concentration (N_D) in the β-Ga$_2$O$_3$ was estimated from the slope of ($1/C^2$) versus V using the equation

$$N_D = -\frac{2}{q\varepsilon\varepsilon_0 A}\left(\frac{dC^{-2}}{dV}\right)^{-1}, \tag{5}$$

where ε = 10 is the dielectric constant of Ga$_2$O$_3$ and ε_0 is the permittivity of free space. The experimental values are very close to those declared by the manufacturer. The parameters calculated from the *I–V* and *C–V* characteristics are summarized in Table I.

The deviation of the ideality factor from unity can be explained by inhomogeneity of the Schottky barrier height or by a contribution by other transport mechanisms to carrier transport. For intermediately doped semiconductors, the current transport can be described by thermionic field emission (TFE). For TFE, the current–voltage relation can be expressed by the following equations:[22]

$$I = I_s \exp\left(\frac{V}{E_0}\right), \tag{6}$$

$$E_0 = E_{00} \coth\left({}^{E_{00}}\!/_{kT}\right) = \eta_{TFE} kT, \tag{7}$$

$$E_{00} = {}^{q\hbar}\!/_{2}\left({}^{N_D}\!/_{m_e^* \varepsilon}\right)^{1/2}, \tag{8}$$

where E_{00} is the tunneling energy, m_e^* is the electron effective mass of β-Ga$_2$O$_3$ ($m_e^* = 0.28 m_0$), and m_0 is the free electron mass.

According to Eq. 7, a theoretical value for the ideality factor (η_{TFE}) can be calculated, which increases to 1.06 and 1.26 when the electron concentration is equal to 1×10^{18} cm^{-3} and 4.4×10^{18} cm^{-3}, respectively. These values are too low to explain the experimental data presented herein. However, the linear relationship between the effective barrier height and the ideality factor for both crystallographic orientations (Fig. 2a)[23,24] as well as the fact that both the ideality factor and effective barrier height are temperature dependent (Fig. 2b)[25,26] indicate that the interface between graphite and β-Ga$_2$O$_3$ is laterally inhomogeneous. Such lateral inhomogeneity is typical for β-Ga$_2$O$_3$[5,27,28] and is related to the presence of defects near the graphite/β-Ga$_2$O$_3$ interface.

The interface trap states in the graphite/β-Ga$_2$O$_3$ Schottky junctions were investigated by frequency-dependent capacitance and conductance measurements.[29] Figure 3 shows the room-temperature capacitance and conductance measured as functions of frequency at zero DC bias. The strong frequency dependence of the capacitance and conductance is caused by the interface states that do not contribute

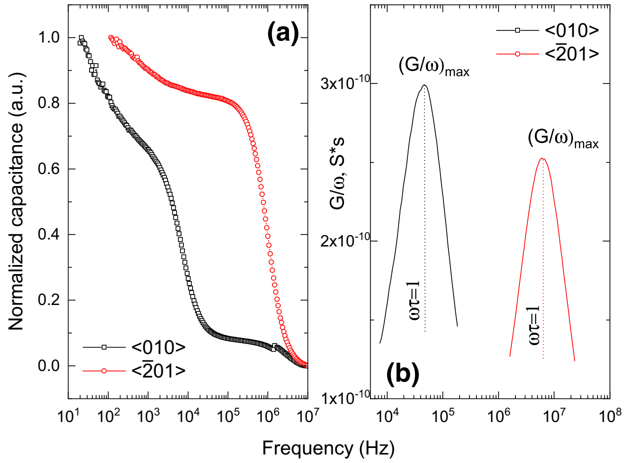

Fig. 3. Capacitance–frequency dependence (a) and conductance-frequency dependence (b) measured at zero bias with 10 mV voltage oscillation for graphite/β-Ga_2O_3 Schottky diodes on Ga_2O_3 substrates with ⟨010⟩ and ⟨$\bar{2}$01⟩ crystallographic orientation.

to the capacitance at high frequencies—the charge at the interface states cannot follow the AC signal due to the finite trapping/detrapping time constant τ. The interface state density N_{SS} and the time constants can be calculated using the Hill–Coleman method from the frequency dependences of the parallel conductance and capacitance as follows:[30]

$$N_{SS} = \frac{2}{qA} \frac{(G/\omega)_{\max}}{\left(\frac{(G/\omega)_{\max}}{C_i}\right)^2 + \left(1 - \frac{C_m}{C_i}\right)^2}, \tag{9}$$

where $\omega = 2\pi f$ is the angular frequency, $(G/\omega)_{\max}$ is the peak value of the conductance on the $(G/\omega) - \omega$ plot (Fig. 3b), C_m is the capacitance corresponding to $(G/\omega)_{\max}$, and C_i is the capacitance of the Ga_2O_3 layer in strong accumulation at high frequency (1 MHz) obtained from C–V measurements. The time constant of the interface traps is given by $\tau = {}^{1}/_{\omega_{\max}}$, where $\omega_{\max}$ is the frequency corresponding to the peak value of the $(G/\omega) - \omega$ plot. All the parameters extracted from the AC measurements are collected in Table I. The frequency-dependent measurements point to the fact that the crystalline anisotropy of β-Ga_2O_3 can significantly affect both the concentration of interface states and the frequency response of graphite/β-Ga_2O_3 Schottky diodes. Better performance of the diodes was observed on ⟨$\bar{2}$01⟩ crystallographic plane due to the better quality of the interface, lower density of interface states, and their shorter time constant.

CONCLUSIONS

The electrical properties of graphite/β-Ga_2O_3 Schottky junctions formed on two different crystallographic planes of β-Ga_2O_3 were investigated. The relationship between the ideality factor and effective barrier height, as well as the fact that both parameters are temperature dependent, revealed the inhomogeneous nature of the Schottky junctions for both ⟨$\bar{2}$01⟩ and ⟨010⟩ crystallographic orientations. Schottky junctions formed on ⟨$\bar{2}$01⟩ crystallographic plane showed lower density of interface states, shorter trapping/detrapping time constants, higher effective barrier height, and lower ideality factor.

ACKNOWLEDGMENTS

This work was supported by Czech Science Foundation Project 17-00546S.

REFERENCES

1. Z. Galazka, *Semicond. Sci. Technol.* 33, 113001 (2018).
2. S.J. Pearton, J. Yang, P.H. CaryIV, F. Ren, J. Kim, M.J. Tadjer, and M.A. Mastro, *Appl. Phys. Rev.* 5, 011301 (2018).
3. Y. Yao, R. Gangireddy, J. Kim, K.K. Das, R.F. Davis, and L.M. Porter, *J. Vac. Sci. Technol. B* 35, 03D113 (2017).
4. E. Farzana, Z. Zhang, P.K. Paul, A.R. Arehart, and S.A. Ringel, *Appl. Phys. Lett.* 110, 202102 (2017).
5. M. Higashiwaki, K. Konishi, K. Sasaki, K. Goto, K. Nomura, Q.T. Thieu, R. Togashi, H. Murakami, Y. Kumagai, B. Monemar, A. Koukitu, A. Kuramata, and S. Yamakoshi, *Appl. Phys. Lett.* 108, 133503 (2016).
6. J. Asanka, C.A. Ayayi, and D. Sarit, *Semicond. Sci. Technol.* 31, 115002 (2016).
7. R. Suzuki, S. Nakagomi, Y. Kokubun, N. Arai, and S. Ohira, *Appl. Phys. Lett.* 94, 222102 (2009).
8. K. Irmscher, Z. Galazka, M. Pietsch, R. Uecker, and R. Fornari, *J. Appl. Phys.* 110, 063720 (2011).
9. K. Sasaki, M. Higashiwaki, A. Kuramata, T. Masui, and S. Yamakoshi, *IEEE Electron Device Lett.* 34, 493–495 (2013).
10. L.J. Brillson and Y. Lu, *J. Appl. Phys.* 109, 121301 (2011).
11. M. Handwerg, R. Mitdank, Z. Galazka, and S.F. Fischer, *Semicond. Sci. Technol.* 31, 125006 (2016).
12. T. Onuma, S. Saito, K. Sasaki, T. Masui, T. Yamaguchi, T. Honda, A. Kuramata, and M. Higashiwaki, *Jpn. J. Appl. Phys.* 55, 1202B2 (2016).
13. T. Matsumoto, M. Aoki, A. Kinoshita, and T. Aono, *Jpn. J. Appl. Phys.* 13, 1578–1582 (1974).
14. N. Ueda, H. Hosono, R. Waseda, and H. Kawazoe, *Appl. Phys. Lett.* 71, 933–935 (1997).
15. K. Makoto, H. Kenji, M. Tomoya, H. Akihiro, O. Takayoshi, O. Toshiyuki, K. Kimiyoshi, S. Kohei, K. Akito, and U. Osamu, *Jpn. J. Appl. Phys.* 55, 1202BB (2016).
16. H. Fu, H. Chen, X. Huang, I. Baranowski, J. Montes, T.H. Yang, and Y. Zhao, *IEEE Trans. Electron Devices* 65, 3507–3513 (2018).
17. L.A. Kosyachenko, R. Yatskiv, N.S. Yurtsenyuk, O.L. Maslyanchuk, and J. Grym, *Semicond. Sci. Technol.* 29, 015006 (2014).
18. R. Yatskiv and J. Grym, *J. Electron. Mater.* 47, 5002–5006 (2018).
19. S. Tiagulskyi, R. Yatskiv, and J. Grym, *J. Electron. Mater.* 47, 4950–4954 (2018).
20. S.M. Sze, *Physics of Semiconductor Devices*, 3rd ed. (Hoboken: Wiley, 2007), p. 815.
21. R. Yatskiv and J. Grym, *Phys. Status Solidi A Appl. Mater.* 214, 1700143 (2017).
22. F.A. Padovani and R. Stratton, *Solid-State Electron.* 9, 695–707 (1966).
23. R.F. Schmitsdorf, T.U. Kampen, and W. Monch, *Surf. Sci.* 324, 249–256 (1995).
24. T.U. Kampen and W. Monch, *Surf. Sci.* 331, 490–495 (1995).
25. A. Hattab, J.L. Perrossier, F. Meyer, M. Barthula, H.J. Osten, and J. Griesche, *Mater. Sci. Eng. B* 89, 284–287 (2002).
26. M.K. Hudait and S.B. Krupanidhi, *Physica B* 307, 125–137 (2001).

27. G. Jian, Q. He, W. Mu, B. Fu, H. Dong, Y. Qin, Y. Zhang, H. Xue, S. Long, Z. Jia, H. Lv, Q. Liu, X. Tao, and M. Liu, *AIP Adv.* 8, 015316 (2018).
28. Q. Feng, Z. Feng, Z. Hu, X. Xing, G. Yan, J. Zhang, Y. Xu, X. Lian, and Y. Hao, *Appl. Phys. Lett.* 112, 072103 (2018).
29. I. Hussain, M.Y. Soomro, N. Bano, O. Nur, and M. Willander, *J. Appl. Phys.* 112, 064506 (2012).
30. W.A. Hill and C.C. Coleman, *Solid-State Electron.* 23, 987–993 (1979).